The Paths of Extratropical Cyclones Associated with Wintertime High-Wind Events in the Northeastern United States*

JAMES F. BOOTH

Department of Earth and Atmospheric Sciences, City College of New York, New York, New York

HARALD E. RIEDER

Wegener Center for Climate and Global Change, and Institute for Geophysics, Astrophysics and Meteorology/Institute of Physics, University of Graz, Graz, Austria, and Lamont–Doherty Earth Observatory, Columbia University, New York, New York

DONG EUN LEE AND YOCHANAN KUSHNIR

Lamont–Doherty Earth Observatory, Columbia University, New York, New York

(Manuscript received 12 December 2014, in final form 11 June 2015)

ABSTRACT

This study analyzes the association between wintertime high-wind events (HWEs) in the northeastern United States and extratropical cyclones. Sustained wind maxima in the daily summary data from the National Climatic Data Center's integrated surface database are analyzed for 1979–2012. For each station, a generalized Pareto distribution is fit to the upper tail of the daily maximum wind speed data, and probabilistic return levels at 1, 3, and 5 yr are derived. Wind events meeting the return-level criteria are termed HWEs. The HWEs occurring on the same day are grouped into simultaneous wind exceedance dates, termed multistation events. In a separate analysis, extratropical cyclones are tracked using ERA-Interim. The multistation events are associated with the extratropical cyclone tracks on the basis of cyclone proximity on the day of the event. The multistation wind events are found to be most often associated with cyclones traveling from southwest to northeast, originating west of the Appalachian Mountains. To quantify the relative frequency of the strong-wind-associated cyclones, the full set of northeastern cyclone tracks is separated on the basis of path, using a crosshairs algorithm designed for this region. The tracks separate into an evenly distributed set of four pathways approaching the northeastern United States: from due west, from the southwest, and from the southeast and storms starting off the coast north of the Carolinas. Using the frequency of the tracks in each of the pathways, it is shown that the storms associated with multistation wind events are most likely to approach the northeastern United States from the southwest.

1. Introduction

A series of recent, costly weather disasters has led to an increased interest in understanding and quantifying severe weather events (e.g., Vose et al. 2014; Kunkel et al. 2013). For the U.S. Northeast, the most frequent cause of extreme wintertime weather is extratropical cyclones, which can create damage through their precipitation (Kunkel et al. 2012) and their winds (Ashley and Black 2008). In view of this, this study seeks to understand the connection between strong wintertime surface wind events and extratropical cyclones in the northeastern United States.

Extratropical cyclones can approach the northeastern United States from the west, from the southwest, and from the south, the latter of which are referred to as northeasters. Several aspects of these wintertime storms have been discussed in the scientific literature. Miller (1946) separated northeasters based on their genesis regions, drawing a distinction between those that originate over the Gulf of Mexico and those that develop over the Atlantic Ocean. Reitan (1974) estimated the

* Supplemental information related to this paper is available at the Journals Online website: http://dx.doi.org/10.1175/JAMC-D-14-0320.1.s1.

Corresponding author address: J. F. Booth, 160 Convent Avenue, Marshak Science Building, Room 106, City College of New York, New York, NY 10031-9101.
E-mail: jbooth@ccny.cuny.edu

DOI: 10.1175/JAMC-D-14-0320.1

most frequent paths of storms for 1951–70, distinguishing paths for storms over the northeastern United States as from the west, from the southwest, from the southeast, and over the ocean [Fig. 12a in Reitan (1974)]. Hirsch et al. (2001) developed a climatology of East Coast winter storms and included a strong wind threshold in their criteria for defining the storms. Dolan and Davis (1992) show that northeasters tend to cause strong beach erosion events because of the westward direction of the winds poleward of the storm center, while Bernhardt and DeGaetano (2012) report on how the North Atlantic Oscillation and El Niño–Southern Oscillation relate to the storms that cause storm surge. However, less attention has been given to storms causing strong wind events over land in the northeastern United States.

Vose et al. (2014) review the trends in wind events in the United States and find that available surface datasets and reanalysis products disagree on the sign of the trend [Fig. 3 in Vose et al. (2014); Pryor et al. (2009)]. Similarly, Knox et al. (2011) review the current understanding of nonconvective wind events and suggest that there is some debate regarding the mechanisms causing high-wind events in extratropical cyclones. For instance, some case studies suggest that downward-momentum mixing associated with tropopause folds may be responsible for high-wind events (HWEs) (e.g., Iacopelli and Knox 2001; Browning 2004), while other case studies find a key forcing from isallobaric winds (e.g., Durkee et al. 2012). However, the sting jet events discussed in Browning (2004) are rare, and the work on case studies over land (Fink et al. 2009; Gatzen et al. 2011; Durkee et al. 2012; Ludwig et al. 2015) suggests a more prominent role for ageostrophic fluxes.

Studies of strong surface wind in regions of the northeastern United States have examined the most likely wind direction during an event. For instance, Niziol and Paone (2000) used station winds in western New York to show that the winds tend to be directed from the southwest to northeast during the strong events. For the Great Lakes region, Lacke et al. (2007) found a similar southwesterly propensity for the wind direction of strong, nonconvective events (identified using weather reports) in which they defined strong events using the National Weather Service (NWS) criteria for high-wind watch or warning (sustained winds greater or equal to $18\,m\,s^{-1}$ for 1 h or a gust greater or equal to $26\,m\,s^{-1}$ for any duration). Lacke et al. (2007) also found that the nonconvective high-wind events occur slightly more often in March and April, as compared to in November–February. Most recently, Pryor et al. (2014) found spatial coherence over distances of up to 1000 km in strong surface wind events, which, as they point out, implies that synoptic systems create the wind events.

For Europe, far more attention has been given to windstorms in the literature, with studies that examine surface observations (Seregina et al. 2014) and reanalysis (Pinto et al. 2007; Leckebusch et al. 2008; Donat et al. 2010; Nissen et al. 2010; Pfahl 2014; Roberts et al. 2014), global climate models (Knippertz et al. 2000; Della-Marta and Pinto 2009), case studies (Fink et al. 2009; Gatzen et al. 2011; Ludwig et al. 2015), and statistical models (Schwierz et al. 2010; Haas and Pinto 2012; Born et al. 2012; Pinto et al. 2012). Leckebusch et al. (2008) developed a method for identifying windstorms in gridded data, termed ''footprinting.'' The technique detects winds that exceed a local threshold and then looks for spatial clusters of exceedances and tracks the clusters in time. Using this method, Leckebusch et al. (2008) established that high-wind events associated with extratropical cyclones tend to occur to the south-southeast of the cyclone center, either along the cold front or slightly ahead of it. Nissen et al. (2010) used the same technique to show that a similar spatial arrangement exists for high-wind events over the Mediterranean. These results for Europe, coupled with the work in the northeastern United States (Niziol and Paone 2000; Lacke et al. 2007), suggest that associating extratropical cyclones with high-wind events in the northeastern United States should identify a predominance of storms with their centers to the north-northwest of the wind events.

With this in mind, the present study will examine northeastern United States strong wind events and associate them with extratropical cyclone tracks. A goal of this work is to test if the results from Europe—that the locations of the strongest winds occur southeast of the storm center—apply in the northeastern United States. We analyze station-based wind data from the daily summaries of the National Oceanic and Atmospheric Administration (NOAA) integrated surface database (ISD; Smith et al. 2011)—a quality-controlled, surface-station dataset. To maximize the likelihood of studying extratropical cyclones, we examine only winds that occur from December through February (DJF).

Our analysis begins with an examination of high-wind events in the northeastern United States and then turns its focus to those storms identified as creating the strong wind events. To categorize the strong wind events, this study uses a probabilistic approach, following Della-Marta and Pinto (2009). Once identified, strong wind events are associated with extratropical cyclone tracks, as for example in Yarnal (1993, chapter 6), to identify the pathway of the storms that are associated with strong winds in the northeastern United States. After identifying the most likely pathway for the storms, we test the robustness of the pathway results.

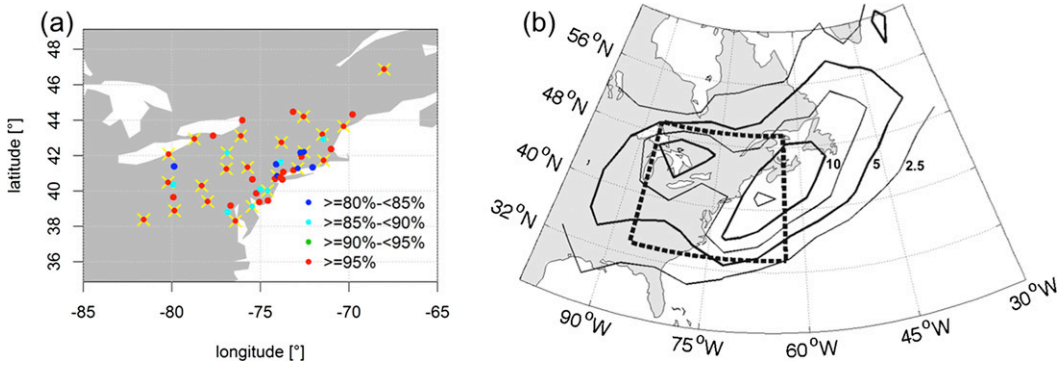

FIG. 1. (a) Stations and (b) track density. In (a), locations of ISD stations in the NOAA Northeast region with at least 80% MAX data for DJF for 1979–2012 are shown. The color of stations corresponds to percentage of data available. Yellow times signs show stations used for repeated analysis in which a set of more evenly spaced stations was used (i.e., one site within a 100-km radius; see text for further explanation). In (b), track density for extratropical cyclones in DJF on the basis of tracks from the Hodges (1999) tracking algorithm is shown [units: count per winter (CPW)]. Contour interval is 2.5 CPW. Thicker contours show 5 and 10 CPW. The black dashed box shows the region through which all tracks must travel to be included in database.

2. Data and methods

a. Data

This study uses the daily summary data from NOAA's ISD. The ISD consists of global, synoptic observations compiled from surface weather observation stations, ranging from airports to military bases. The daily summary dataset is a quality-controlled subset of the ISD provided by NOAA. The key variable we examine is the sustained wind maximum, which NOAA defines as the daily maximum of the 2-min averages from each hourly observation reported for the day (M. Lackey, NOAA, 2014, personal communication). Here we refer to this variable as MAX. We focus the analysis on the sustained wind maximum rather than the wind gust because the MAX data are more frequently available for our study period and region. We also use the daily mean wind speed (MEAN), defined as the 24-h average wind speed, which is also provided as part of the daily summary. The data are reported in whole knots, which results in the data being quantized (with an approximate interval of 0.5 m s^{-1}) rather than continuous (Pryor et al. 2009). We note that the daily summary dataset does not include wind direction, and therefore it is not considered in this study.

Our analysis focuses on the Northeast region as defined by NOAA, which consists of 12 states: West Virginia, Maryland, Pennsylvania, Delaware, New Jersey, New York, Connecticut, Rhode Island, Massachusetts, Vermont, New Hampshire, and Maine. For these states, we use all of the ISD stations for which at least 80% of MAX data are reported during DJF for the period from January 1979 to December 2012, which yields 49 stations (Fig. 1a). We choose January 1979 as the start date for our analysis because it coincides with the beginning of the reanalysis data used to identify extratropical cyclones (see section 2c). A table that lists all station names, station locations, and the percentage of data available is provided in the supplementary material (Table S1).

We choose a cutoff of 80% data coverage to establish broad station coverage over the entire study region, which allows for a synoptic-scale analysis. To test that this amount of data coverage yields robust results, we performed two sensitivity analyses: 1) we repeated the main analysis reported in section 3 using only stations with 90% or more data coverage, and 2) we tested if data are missing at a given station more often when a high-wind event occurs at one or multiple other stations within 250 km. Neither analysis indicated a systematic bias, suggesting that this set of 49 stations provides a representative synoptic view for winds in the northeastern United States.

Before analyzing the data, we took additional steps to address other potential biases. First, we removed any sustained wind maximum data for which the concurrent mean wind speed data are zero (dubious data). Second, any sustained wind maxima that were found to be suspiciously larger than the concurrent mean wind for that day have been removed. To accomplish this, we define a new variable η for each station i:

$$\eta_i(t) = \frac{\mathrm{MAX}_i(t) - \mathrm{MEAN}_i(t)}{\sum_{j=1}^{N} \mathrm{MAX}_j(t) - \mathrm{MEAN}_j(t)}. \quad (1)$$

In the denominator, we average over the N stations within 250 km of station i, not including station i. If η is

large, then the difference between the MAX and MEAN at station i is large, as compared with the difference between MAX and MEAN for the surrounding stations. We chose to remove any data for which η was larger than 4, which led to a removal of overall less than 0.002% of the original data, or 172 total data points.

The data removed using the η threshold are, by definition of η, isolated wind events. However, some of the data removed are strong winds, which might suggest that this method is removing important data. However, 168 of the 172 WMAX data removed using η occur prior to 1 January 1999 (Fig. S1 of the supplemental material). This date corresponds to the near completion of the transition to the ASOS observing systems (McKee et al. 2000), which meant the majority of the manual reporting was replaced by electronic reporting. McKee et al. (2000) note that the speed and direction were similar for manual and ASOS, but there were issues with the gust measurements as a result of differences in the measurement-averaging window of the devices. Hayes and Kuhl (1995) note a difference in the reporting of peak-wind events due to differences in thresholds for defining peak winds. These biases would not affect our results because we do not focus on gusts or the count of peak-wind reports. On the other hand, the fact that such a high percentage of data identified using η occurred prior to 1999 suggests that the data removed because $\eta > 4$ may indeed be erroneous. For our purposes of associating multistation wind events with extratropical cyclones, the removal of the data with large η is justified.

b. *Identifying HWEs*

The classification of HWEs that will be utilized in this study is a probabilistic approach following statistical extreme value theory (EVT) (e.g., Coles 2001; Coles and Pericchi 2003; Davison and Smith 1990). For the identification of HWEs we use a peak-over-threshold (POT) model for MAX, based on the generalized Pareto distribution (GPD). Asymptotic arguments (e.g., Pickands 1975) justify the use of the GPD for modeling exceedances over a high (enough) threshold because the GPD is the limiting distribution of a normalized exceedance over a threshold as the threshold approaches the maximum of the distribution (e.g., Coles 2001). The GPD is defined as

$$F(x) = 1 - \left(1 + \xi\frac{x-\mu}{\sigma}\right)^{-(1/\xi)},$$
$$\sigma > 0, \quad x > \mu, \quad 1 + \xi\frac{x-\mu}{\sigma} > 0, \tag{2}$$

where x are daily data (here MAX), u is the threshold value, and σ and ξ are the scale (a measure of the spread of the distribution of x) and shape parameter (which is determining the shape of the distribution rather than shifting it as u does or shrinking/stretching it as σ does), respectively. In the GPD framework an essential step is to determine a threshold u for which the asymptotic GPD approximation holds. Threshold choice involves a trade-off between bias and variance as (i) a too-high threshold will reduce the number of exceedances and increase the estimation variance, while (ii) a too-low threshold will induce a bias as the GPD will poorly fit the exceedances.

In this study we use the POT package (Ribatet 2007) within R for the EVT analysis. In this package the GPD parameters (σ and ξ) are computed by maximum-likelihood estimation. Evaluation of the GPD fit at the 49 Northeast U.S. sites considered here show that the 97th quantile provides a suitable threshold choice at all sites, satisfying the trade-off between bias and variance. Figure S2 of the supplemental material provides an exemplary comparison of results from GPD fits at selected sites with too-high and too-low threshold values.

Figure S3 of the supplemental material shows the probability density functions (PDFs) of wintertime MAX from the 49 Northeast U.S. sites in the ISD that fulfill the data selection criteria outlined in section 2a. The PDFs are asymmetric with heavier upper tails. We note that a similar skew was found in the PDFs of surface winds using the entire year, rather than DJF (He et al. 2010), and similar statistics were found in Pryor et al. (2014). Figure S3 also shows that the winds exceeding the threshold for a high-wind watch or warning for the NWS (days with MAX $> 18\,\mathrm{m\,s^{-1}}$) represent the upper end of the PDF range and occur very rarely.

Next we analyze the winds from two stations to illustrate why we have chosen to use probabilistic statistics. Figures 2a,b show the observed MAX (y axis) versus the estimate from a Gaussian fit (x axis) for two selected (and representative) sites in the northeastern United States: Bridgeport, Connecticut (left column), and Elkins–Randolph County, West Virginia (right column). The figures confirm that the tails of MAX are non-Gaussian (i.e., data from a Gaussian distribution would lie close to the diagonal 1:1 line). The gray-hashed boxes in Figs. 2a,b give the data range at the two selected sites beyond the 97th quantile. Figures 2c,d (which are a zoom-in on the gray-hashed boxes of Figs. 2a,b) show observed (y axis) versus GPD-fitted (x axis) MAX. Comparing Figs. 2a,b with Figs. 2c,d shows that the GPD provides a better fit than does a Gaussian distribution.

After fitting the GPD ($F_{\xi,\mu,\sigma}$), we calculate the empirical return level R_T as

$$R_T = F^{-1}_{\xi,\mu,\sigma}\left(1 - \frac{1}{T}\right). \tag{3}$$

Return levels are of practical interest because they describe the probability of exceeding a value x within a

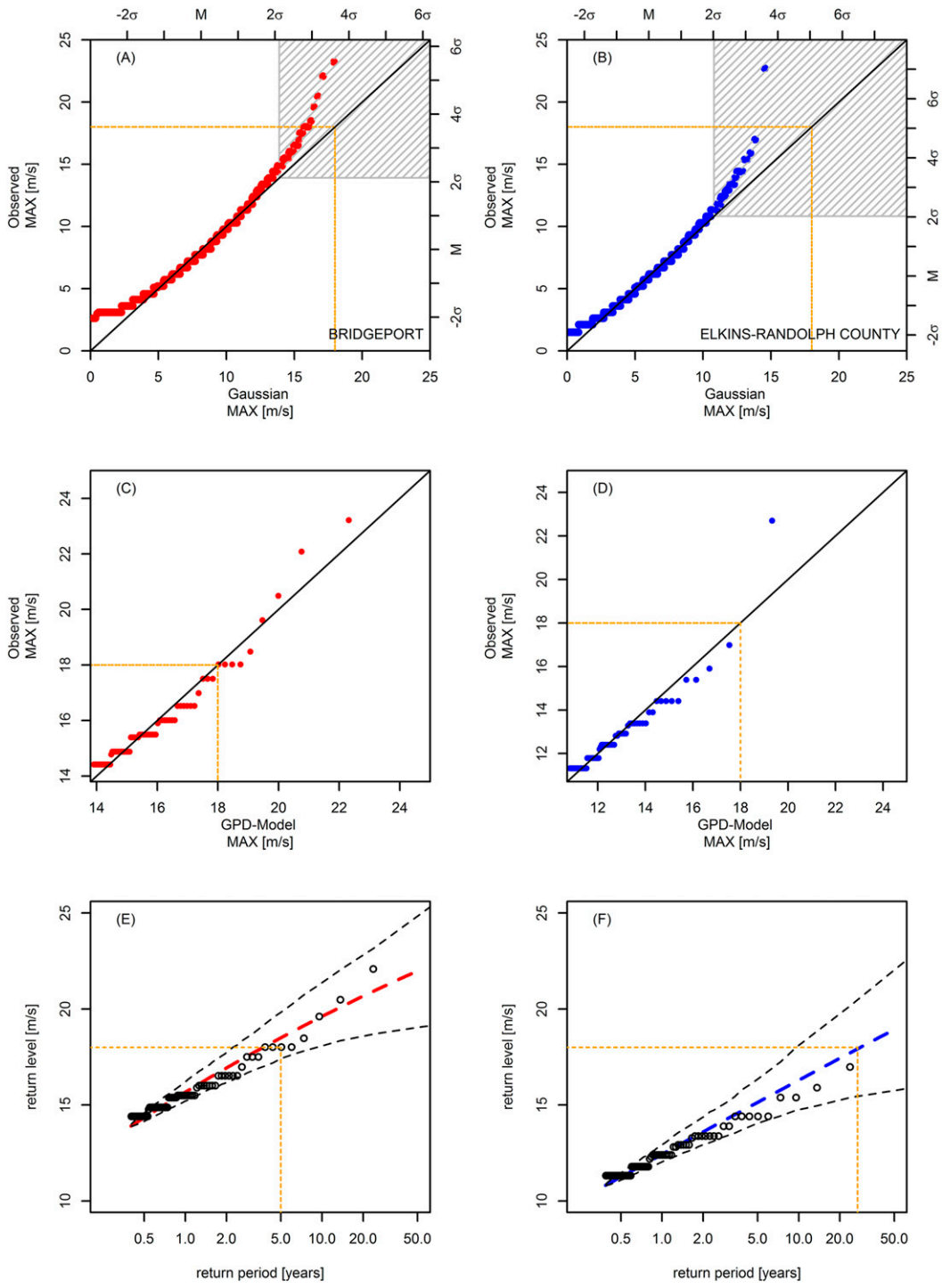

FIG. 2. (a) Quantile–quantile (QQ) plot comparing observed MAX ($m\,s^{-1}$) at Bridgeport with a least squares fitted Gaussian. (b) As in (a), but for Elkins–Randolph County. (c) QQ plot comparing observed MAX from Bridgeport with GPD-fitted MAX. (d) As in (c), but for Elkins–Randolph County. (e) Return-level plot for Bridgeport from the fitted GPD in (c). (f) As in (e), but for Elkins–Randolph County. Gray-hashed boxes in (a) and (b) mark the data range above the 97th quantile at each site. Orange dashed lines mark the NWS threshold for a high-wind watch or warning (i.e., $18\,m\,s^{-1}$) in all panels. Secondary axes in (a) and (b) show corresponding mean values (M) and standard deviations (σ). The black dashed lines in (e) and (f) show the 95% confidence intervals.

time window T. Figures 2e,f show return-level plots for the two selected sites. Thus, for example, MAX $> 18\,\mathrm{m\,s^{-1}}$ at the Bridgeport site would have a probabilistic 5-yr return level, while at the Elkins–Randolph County site it would have a probabilistic return level of more than 20 yr.

For the purpose of this study we choose to use 1-, 3-, and 5-yr return levels to define HWEs. The reason is twofold: (i) return levels accurately capture the tail properties of MAX, and (ii) they provide a comparable standardized metric for MAX across individual sites. Using HWEs at each station, we identify simultaneous exceedances of multiple station return levels (herein, multistation events) by finding all HWEs that occur on the same date ±1 day. The window of ±1 day accounts for the possibility that a storm caused HWEs on either side of 0000 UTC (i.e., two different days in the daily summary) and the possibility of the same storm transiting the study region over a 2-day period. We define the center of a multistation event as the average of latitude and longitude positions of the stations reporting the event.

c. *Extratropical cyclone association*

Extratropical cyclones are identified by tracking their low-pressure centers, using 6-hourly sea level pressure (SLP) fields from the ERA-Interim (Dee et al. 2011). ERA-Interim has been shown to compare favorably to other reanalysis data for cyclone tracking (Hodges et al. 2011). To account for possible biases in the trackers (e.g., Neu et al. 2013), we performed our analysis using two separate cyclone-tracking algorithms: that of Hodges (1999) and the Bauer and Del Genio (2006) climatology for midlatitude storminess. Despite major differences in the design of the tracking algorithms, we found similar results in the wind analysis for both. Therefore we present in the remainder of the paper only results based on the Hodges tracking scheme.

For the track database, we include tracks that last for at least 48 h and travel at least 1000 km, which allows focusing on mobile synoptic systems. Figure 1b shows the track density for all storms that pass through a box over the Northeast region (Fig. 1b; black, dashed box). The box used is sufficiently larger than the region of the stations so that the storm set includes all storms that might influence the area. The track density is a count of the tracks per 2° by 2° grid box per winter (DJF). The pattern shows a maximum over the Gulf Stream and a secondary maximum over the Great Lakes, in good agreement with the pattern reported for East Coast wintertime storms in previous work (Hirsch et al. 2001). For DJF, from 1979 to 2012, for tracks passing through the box in Fig. 1b, we find a total of 1034 storms.

To associate the cyclone tracks with multistation wind events, we require that the cyclone center be within 1500 km of the geographical center of the event (see end of section 2b for the definition of a center of a multistation event). We have tested other radii (e.g., 1000 km) and found that the smaller distance excludes obvious storms. Since the track data are 6 hourly, while the station data are daily, we consider any cyclone that is within 1500 km at the time of the event ±12 h. For the multistation events that occur on a single day, we use 1200 UTC for that day. For the events that span two days, 0000 UTC on the latter day is used.

In the cases in which multiple storms are found in proximity (in time and space) of the wind event, wind direction data from the ERA-Interim are used to identify the most likely related storm. For this, first the area average of the 925-hPa zonal and meridional winds over a 5° by 5° region centered on the multistation event is calculated. Second, wind direction is calculated from the area-averaged winds. If the wind direction has a northerly component, we retain the cyclones east of the station event (i.e., the winds are part of the back end of the storm), and vice versa for winds with a southerly component. For the rare case that there are still multiple storms that fulfill the selection criteria, the storm that is closest in space to the wind event is kept.

3. Results

a. *Extratropical cyclone tracks for multistation HWEs*

The HWEs during DJF in the northeastern United States are defined by identifying wind events that exceed the station-specific 1-, 3-, and 5-yr return levels (Table 1). We then find the dates on which multiple stations have HWEs. Table 1 shows the results for exceedances of the 1-, 3-, and 5-yr return levels, with the number of events occurring simultaneously at multiple stations decreasing as the number of stations increases, though not monotonically. The analysis that follows will mainly focus on multistation events for which three or more stations exceed their 3-yr return levels. There are 52 of these events (i.e., 13 + 8 + 6 + 8 + 17, using the data on the 3-yr return-level row in Table 1). Analysis will also be carried out on multistation events for which five or more stations exceed their 5-yr return periods, for which there are 15 events (i.e., 6 + 4 + 5, using the data on the 5-yr return-level row in Table 1).

Isolated events are defined as the dates for which only one station exceeds the given return level, and these occur most frequently. As shown in column 3 of Table 1, the occurrence of isolated events greatly decreases if 1-yr

TABLE 1. Count of HWEs and multistation events.

Return level (yr)	Total HWEs	Isolated events (isolated at 1-yr RL)	Multistation events on the same day by number of stations[a]						
			Two	Three	Four	Five	Six	Seven or more	Max no. of stations
1	1621	172	58	42	24	18	22	62	29
3	490	116 (47)	27	13	8	6	8	17	14
5	289	85 (28)	16	11	10	6	4	5	8

[a] For each of the return levels, the count of multistation events per number of stations does not monotonically decrease as the number of station increases. It does have a downward tendency; however, it also has a long tail, as indicated by the last column.

return levels for surrounding stations are considered. For example, if the simultaneous exceedances of 5-yr return levels are considered, then 85 single-station exceedances of the 5-yr levels are found. However, if we consider simultaneous exceedances of 1- and 5-yr levels, the number of single-station exceedances of the 5-yr levels drops significantly, down to 28. For reference, the dates for multistation events defined as five or more stations with exceedances of the 5-yr levels are listed in Table S2 of the supplemental material. Some of these storms were deadly (see, e.g., Asuma 2010).

Using the extratropical cyclone association technique described in section 2c, we associate each multistation event with a cyclone track, when possible. Figure 3 shows examples of this for multistation events in which three stations simultaneously experienced winds that exceeded their 3-yr return levels (Table 1). In this case, cyclones were associated with 11 of the 13 multistation events. The figure shows that in some cases a multistation event is based on three stations in close proximity (e.g., 21 December 2012 in Fig. 3b), while in other cases the stations are spread across the region (e.g., 29 December 1994 in Fig. 3a).

Next, we examine the associated tracks when using different thresholds to define a multistation event (Fig. 4). Figure 4a shows the tracks for all events for which there are at least five stations at which the wind exceeded the station's 1-yr return level. There are 102 multistation events that fit the definition, and for 82 of these events an associated cyclone is identified. In this case, no preferred path is obvious, perhaps because of the large number of tracks included in the plot. Figure 4b shows the paths for multistation events defined as exceedances of the 3-yr return level at three or more stations. There are 52 events that fit this definition, and for 44 of these events an associated cyclone is identified. In this case, there appear to be more storms that arrive in the Northeast region from the west or southwest. Figures 4c and 4d show results for more stringent definitions of multistation events, and a higher percentage of events are associated with a cyclone track that arrives in the northeast from the southwest. For the multistation events defined as five or more stations exceeding their 3-yr return level, 31 events are found with 26 associated cyclone tracks. For the multistation events defined as five or more stations exceeding their 5-yr return level, 15 events are found with 13 associated cyclones identified.

Figure 5 shows, for different thresholds used to define a multistation event, the location of the storm center (in red) and the location of the average of the latitude and longitude for the stations with HWEs in the

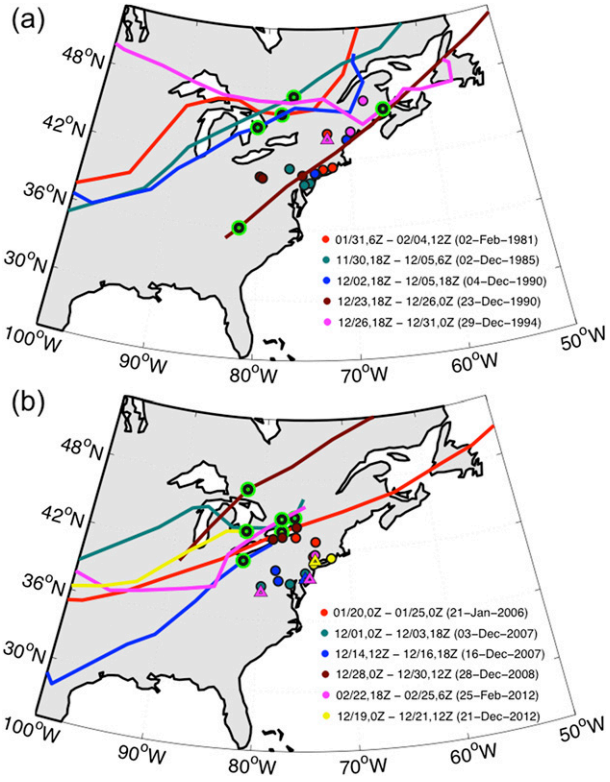

FIG. 3. Multistation events and associated track examples: multistation events for which the winds exceed 3-yr return levels at exactly three stations. For this criterion, 13 multistation events were identified. For 11 of these events, an associated extratropical cyclone is identified. Cyclone tracks are the lines; station locations are the dots. The associated tracks and stations are given in the same color. The green dot on each track shows the location of the storm at the date of the multistation event. The legend shows the full date extent of each track and the date of the multistation event in parentheses. For the 4 Dec 1990 case, there are two stations in the New York City region that nearly overlap.

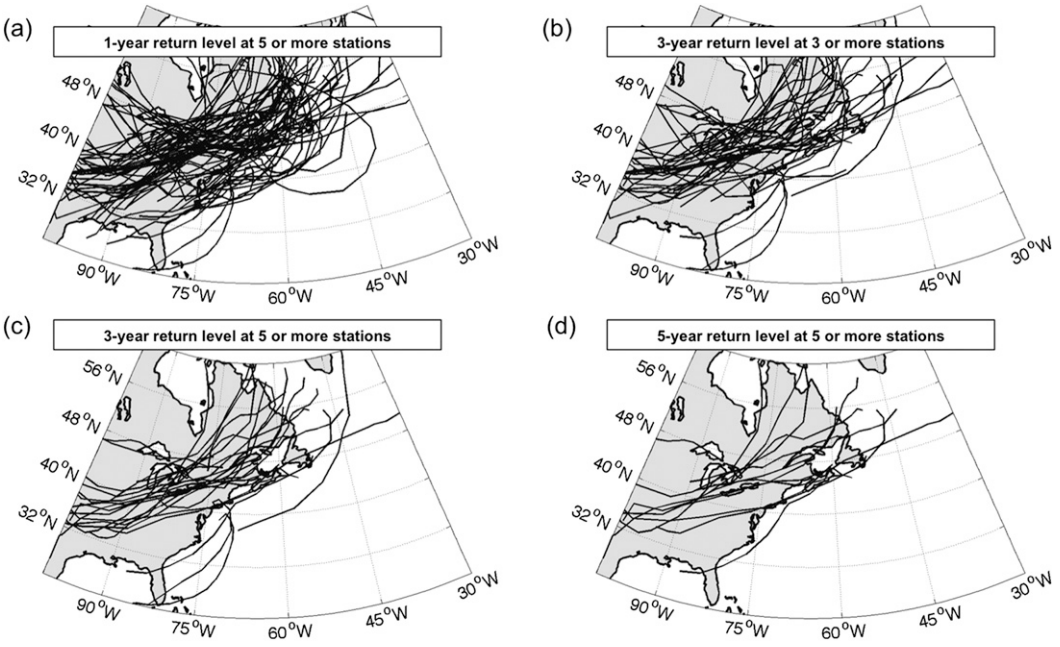

FIG. 4. Track associated with multistation events based on different criteria: (a) 1-yr return level (RL) at five or more stations—track count: 84 (total events: 102), (b) 3-yr RL at three or more stations—track count: 44 (total events: 52), (c) 3-yr RL at five or more stations—track count: 26 (total events: 31), and (d) 5-yr RL at five or more stations—track count: 13 (total events: 15). Track count gives the number of associated tracks, and total events gives the number of multistation events identified for each specified criterion.

event (in blue). For each of these definitions, the majority of the storm centers are north or northwest of the stations experiencing a wind event, suggesting that the winds are in the south-southeast quadrant of the cyclones. Consistent with this result, a composite of the SLP field for the study domain (using ERA-Interim) on the day of the multistation events, based on five or more stations exceeding the 5-yr return levels, also shows the storm center north of our study region (Fig. 6). The SLP contours further suggest that the winds are directed from the southwest to the northeast, which is in agreement with the individual station studies of Niziol and Paone (2000) and Lacke et al. (2007).

b. *Quantifying the preferred extratropical cyclone path*

The qualitative results from the previous section show a preference for the multistation events being caused by storms approaching from the southwest. Next, we quantify this preference by examining the relative occurrence of strong-wind-associated storms arriving from different directions. To do this, a new methodology for separating

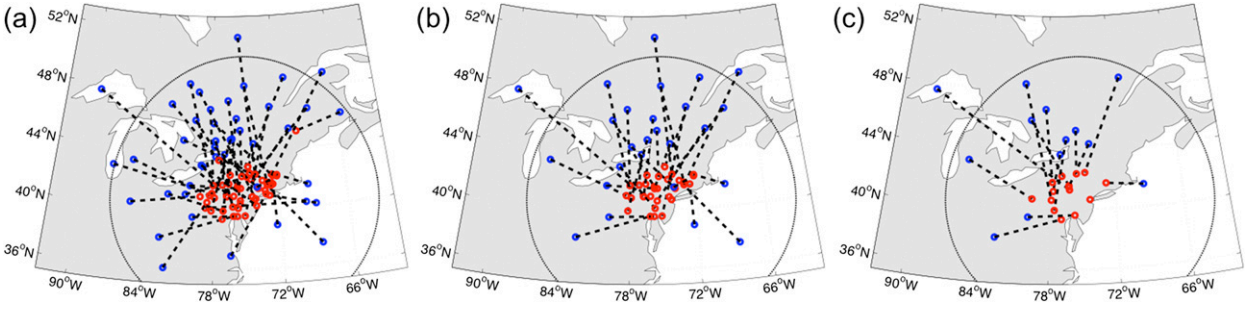

FIG. 5. Location of cyclone centers (blue) and geographical average location of associated stations (red) during multistation events with (a) 3-yr RL at three or more stations, (b) 3-yr RL at five or more stations, and (c) 5-yr RL at five or more stations. Dashed black lines connect the station center to the associated storm center. For reference, the black circle shows a distance of 1000 km from the geographical center of all of the stations.

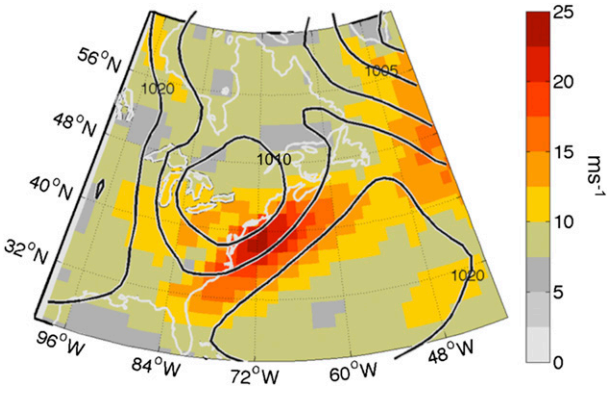

FIG. 6. Composite for multistation events. Contours show SLP (hPa), and shading shows wind speed at 925 hPa ($m\,s^{-1}$). Multistation events here are defined as HWEs exceeding the 5-yr return level at five or more stations.

the cyclone tracks based on their initial locations and paths is presented. Then the technique is applied to all cyclone tracks in the northeastern United States and to the tracks associated with multistation events.

Motivated by the track separation presented in Reitan (1974), we have designed an analysis aimed at separating the cyclone tracks into those that take a zonal path toward the northeastern United States, those that arrive from the southwest and those that move northward along the coast. The analysis utilizes knowledge of the tracks' initial development region and their trajectory across the northeastern United States. We use a reference frame centered at the geometric average of the latitude and longitude positions of the 49 weather stations to draw a crosshair based on fixed lines of latitude (41.37°N) and longitude (75.06°W), which herein are referred to as latFIX and lonFIX for simplicity. The storms are then separated into four groups:

1) fromNW: tracks that begin northwest of the intersection and remain north of latFIX,
2) fromSW: tracks that begin southwest of the intersection and either remain in that quadrant or cross latFIX traveling north to the west of lonFIX,
3) fromSE: tracks that cross lonFIX traveling east to the south of latFIX, and
4) overOCEAN: tracks that remain east of lonFIX or cross lonFIX traveling west.

We note that many of the storms in the fromSE and overOCEAN tracks could be considered northeasters based on the wind pattern they generate when passing the northeastern United States. However, the classification used here does not include northeasters as an individual category because the paths have been separated based on their origin.

Figures 7a–d show the track density (using the same procedure as in Fig. 1b) for the full storm set based on these categories. For this separation, we find that if we consider all events there is a relatively equal number of tracks per characteristic path (Table 2). To test the sensitivity of the separation in respect to the values of lonFIX and latFIX, we repeat the analysis, shifting the location of the reference frame center by 1° in each direction (Table 2). As expected the results show that counts change with shifts; however, this does not result in any drastic changes.

Next the track separation technique is used to parse the tracks associated with the multistation events. For this analysis, we use the tracks found based on events for which the winds exceed the 3-yr return level at three or more stations (i.e., Fig. 4b). Figures 7e–h show these tracks separated into the characteristic pathways, with the counts as follows: fromNW (7), fromSW (27), fromSE (9), and overOCEAN (1). Using the number of total storms per characteristic track found (given in Table 2), the relative frequency of storms causing multistation events per characteristic path is calculated. For fromSW the value is 10.5%, which is at least 3 times greater than any of the frequencies for the other pathways. Furthermore, given that the four pathways have nearly the same number of tracks when all of the extratropical cyclones are considered (Table 2), we can use binomial probabilities to test the significance of the strong wind path result. In particular, if we consider this a Bernoulli experiment and use the binomial distribution to test the likelihood of 27 of the 44 events coming from one pathway, the probability is $<1 \times 10^{-6}$.

To conclude this section, we discuss our choice for extratropical pathway separation. The crosshair separation technique used is subjective and based on prior understanding of the likely pathways that storms take to arrive in the northeastern United States (e.g., Reitan 1974). In an attempt to make a more objective track separation, the tracks separated were also using hierarchical clustering (Ward 1963), a technique that has been previously applied to atmospheric circulation regimes (e.g., Casola and Wallace 2007). The clustering analysis resulted in a similar set of final clusters (i.e., the characteristic paths) as those we found using the crosshair. However, the number of tracks per final cluster was very sensitive to the geographical extent of the tracks that was fed into the clustering algorithm. The clustering algorithm does not provide a simple mechanism for showing the sensitivity of the track separation to slight changes in the method, as we did here for the crosshair method with Table 2. This led us to conclude that our technique, though subjective, offers the simplest and most easily reproducible method for separating the tracks.

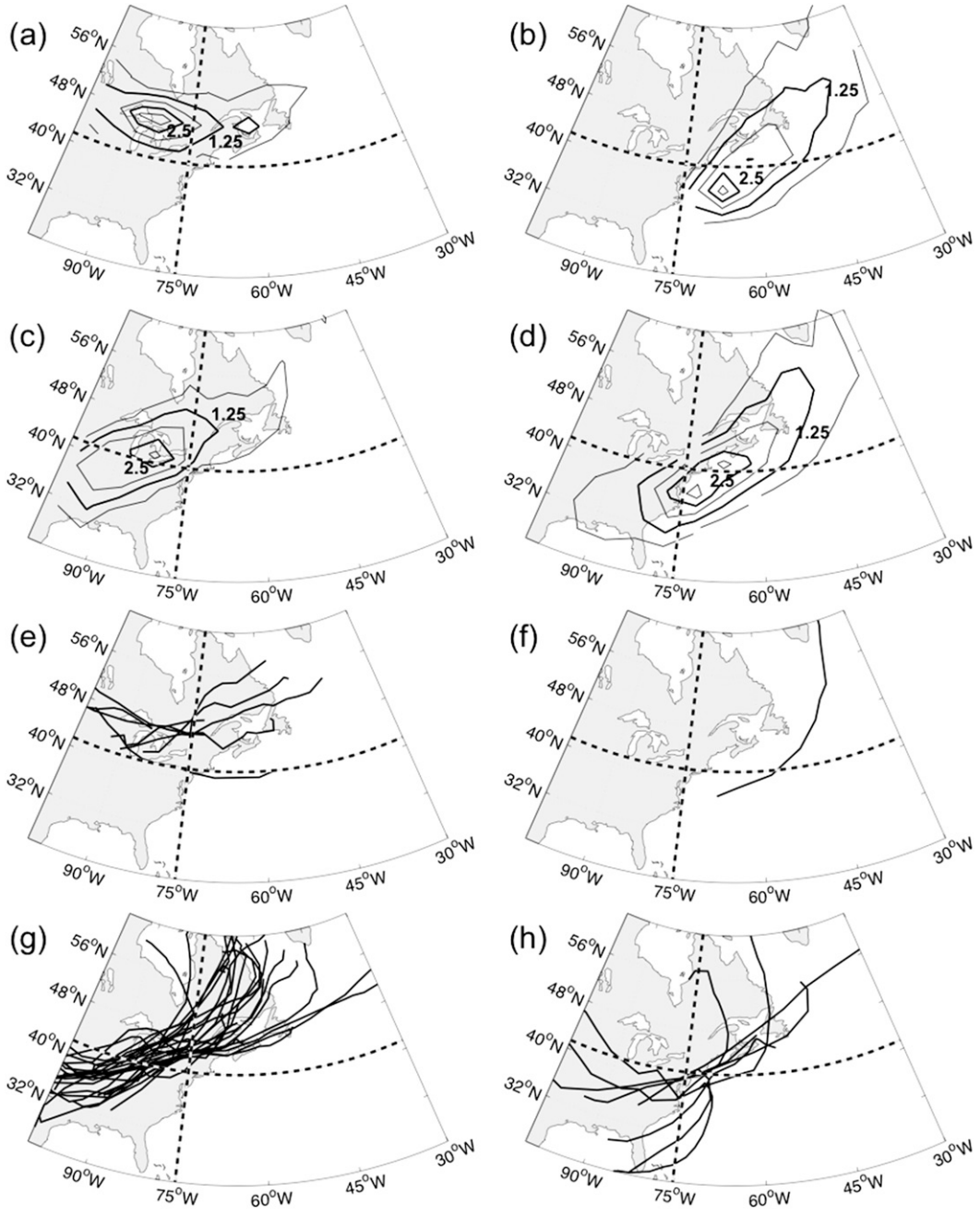

FIG. 7. Separating tracks based on characteristic pathways: (top and top middle) track density for all tracks and (bottom middle and bottom) track paths for storms associated with multistation events. Pathway names: (a) fromNW, (b) overOCEAN, (c) fromSW, and (d) fromSE. Contour interval in (a)–(d): thin lines indicate 1.25 CPW; thick lines indicate 2.5 CPW. For storms associated with multistation events, track count per path: (e) 7, (f) 1, (g) 27, and (h) 8. Multistation events are defined here as three or more stations exceeding their 3-yr return level. Dashed lines show crosshairs designated by the geometric-mean latitude and longitude of the stations.

c. Robustness of the preferred extratropical cyclone path

This section details two analyses designed to test the robustness of the preferred pathway result. First, the sensitivity of the pathway analysis to the geographical density of the surface stations is evaluated. Second, we test if the pathway analysis is sensitive to the number of stations within range of the cyclone winds.

TABLE 2. Track counts per characteristic paths vs location of crosshair counts are listed as fromNW/fromSW/fromSE/overOCEAN.

	40.4°N	41.4°N	42.4°N
283.8°W	239/254/240/301	221/256/256/301	201/255/277/301
284.8°W	245/259/264/266	225/258/285/266	205/263/300/266
285.8°W	249/265/279/243	228/260/303/243	207/267/317/243

To test if the existence of a denser concentration of stations along the coast versus inland (see Fig. 1a) creates a bias, we repeat the storm association analysis using a subset of stations that are more evenly spaced. To this aim we retain only one station separated by a 100-km radius, which results in a subset of 23 stations (Fig. 1a; yellow crosses). Using the 23-station subset, we find 27 multistation events defined based on at least a 3-yr return level at three or more stations (as opposed to the 52 multistation events found using the full set). For these 27 events, we find 23 associated tracks, and the track separation of the storms again results in fromSW being the most likely pathway (supplemental Fig. S4). For further sensitivity analysis we repeated the analysis using radii of 50 and 150 km (to create more regularly spaced station datasets) and found results consistent with those presented based on the 100-km radius. Thus, the results show that the geographical density of stations does not affect our results.

Given the location of the stations relative to the paths of the cyclone centers, one could argue that the fromSW pathway is the most likely to cause multistation events because there are more stations within range of the cyclone winds that take this path. To test this hypothesis, we repeat the track association analysis using HWEs identified in the wind field in the ERA-Interim using a fixed location. The idea behind this analysis is to utilize the temporal and spatial continuity of the reanalysis data in order to identify high-wind events similar to the scale found using the multistation approach at a single, fixed location.

For the region within 77.5°–70°W by 40°–43°N (red box in Fig. 8a), the three strongest values of the 925-hPa daily averaged wind speed from ERA-Interim are identified and averaged to a single value. Then the DJF values in the resulting time series are fit to a GPD. Because the 925-hPa daily averaged wind speed represents a smoother distribution with less striking extremes compared to the ISD observations, we focus on shorter return levels (i.e., 1 yr or above) to establish robust statistics. We identify the high-wind events as those that exceed the 1-yr return level and then isolate events that are at least 3 days apart (to remove the chance of double counting a storm). If multiple exceedances of the 1-yr return level occur within 3 days, the strongest event is used. These HWEs are then associated with extratropical cyclones using the method described in section 2c.

Figure 8a shows the tracks associated with 925-hPa HWEs using the black box shown in the figure. In this case, as for the ISD multistation events, most of the tracks travel from the southwest. To test if this characteristic pathway is caused by coastline geometry or topography, we repeat the analysis using two other boxes at the same latitude, east of the first box (Figs. 8b,c). In these cases we test for associated storms using a set of cyclone tracks that includes more storms over the ocean, which are not necessarily included in the original set of 1034 storms. Once again, the tracks that create high-wind events for each region tend to be those that approach the box from the southwest. These results suggest that the identification of the fromSW pathway in the station analysis is unlikely to be based on which track passed over the most stations. These results also have implications for the cause of the fromSW pathway being the dominant track for wind events in the Northeast, related to the location within cyclones where the strongest winds occur. This is discussed in section 4.

d. *Geographical distribution of high-wind return levels*

For the EVT-based HWEs, we also examine the geographical climatology of events in the northeastern

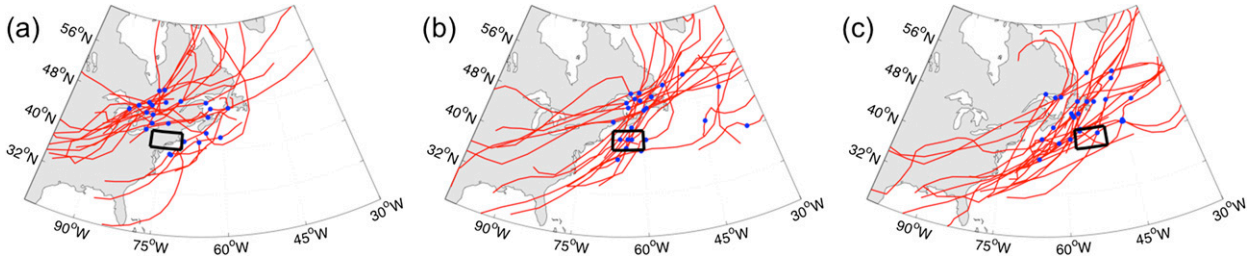

FIG. 8. Cyclone track association for area average of 925-hPa reanalysis winds in the black rectangles. Latitude range for all boxes: 40°–43°N. Longitude ranges: (a) 77.5°–70°W, (b) 67.5°–60°W, and (c) 57.5°–50°W. Red lines indicate the cyclone tracks, and blue dots mark the location of the cyclone at the time of association with a high-wind event for the area-averaged wind in the box.

United States by plotting the average wind speeds for the 1-, 3- and 5-yr events for each station (Fig. 9). Figures 9a–c show that the average strength of HWEs at stations near the Great Lakes and stations along the coast are usually larger than those for inland stations. Given the results from Fig. 9, we use the geographical locations of the stations to create four subsets of sites for the northeast: Great Lakes, inland, near coast, and at coast (Fig. 9; Table S1 in the supplemental material gives each station's designation). Station designation is defined in the following way. The Great Lakes stations are all stations within 100 km of any Great Lake. The at-coast stations are all stations within 40 km of the coastline, while all stations between 100 and 40 km from the coastline are classified as near coast. We then calculate average wind speeds for the 1-, 3- and 5-yr events for each of the subsets. The results show that winds are stronger near the Great Lakes and at the coast. A detailed summary is presented in Table 3 serving as a first-order benchmark for the strength of wintertime high-wind events in these regions of the northeast. We note that the distances used to separate the data are arbitrary and chosen to simplify the presentation in Table 3.

4. Discussion

The analysis reveals that storms taking a path from the southwest toward the northeast region are most likely to cause multistation strong wind events in the region (Fig. 4). It appears that this is a result of the south-southeast quadrant of these storms being more likely to pass over the stations as compared with any of the other paths, as evidenced by the fixed-location analysis of the reanalysis winds (Fig. 8). Figure 8 also shows that if we consider a region farther east, the dominant storms would be those from the fromSE or fromSW categories for our 1034 storms. This, again, is because the east-southeast quadrant of those storms would be more likely to pass over that region. As such, our work does not imply that the fromSW storms create stronger winds than storms from the other groups but that the strong winds generated by the storms taking the fromSW path are most likely to occur over the northeastern United States. This is consistent with an analysis of strong-wind-producing storms over western Europe (Ulbrich et al. 2001; Leckebusch et al. 2008; Nissen et al. 2010; Pfahl 2014), which finds that the cyclone centers tend to be north of the wind events and that the wind events tend to be in the warm sector near the cold front or just behind the cold front. The locations of the strong winds relative to the storm center also agree with composite views of winds within extratropical cyclones (e.g., Bengtsson et al. 2009; Catto et al. 2010; Booth et al. 2013).

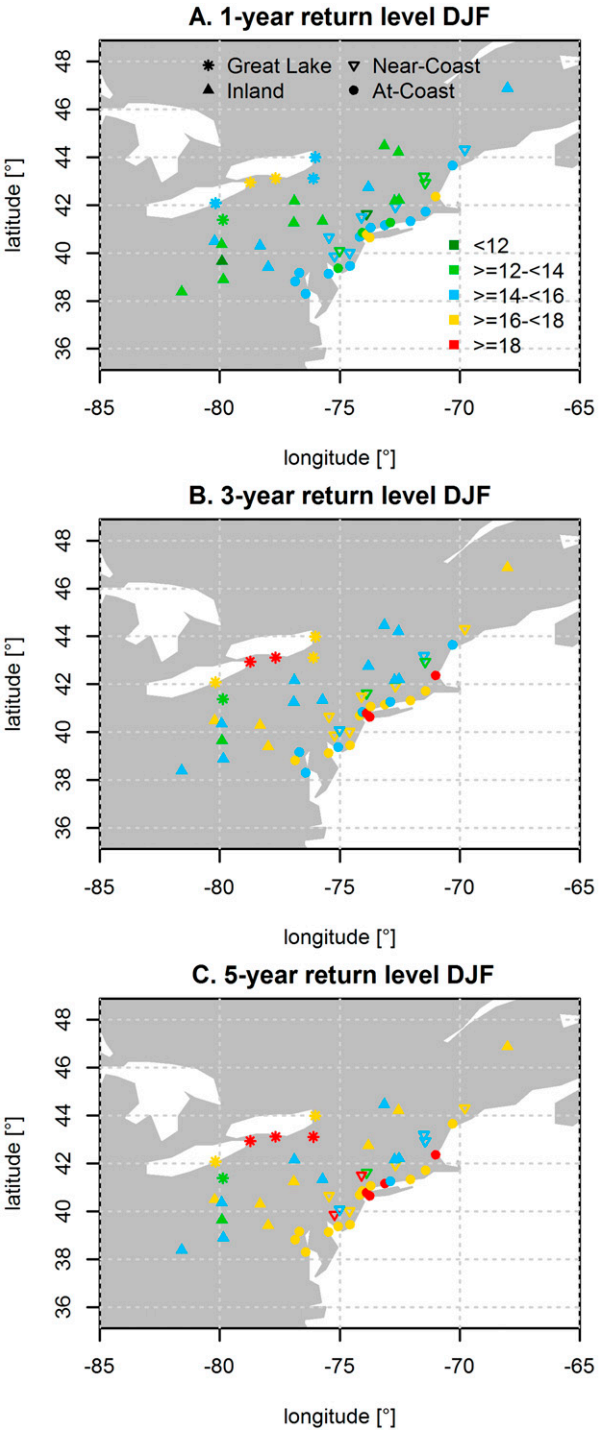

FIG. 9. (a) The 1-yr MAX return level on a site basis. (b)–(c) As in (a), but for 3- and 5-yr return levels.

We also tested for a relationship between the strength of the wind events and the strength of the storms, based on the storm-centered SLP gradient (gradSLP), for each storm at the time of the wind event. In an analysis of the set of multistation events for which the 3-yr return levels

TABLE 3. Average strength of wind events by region MIN/MEAN/MAX ($m\,s^{-1}$).

	Great Lakes	Inland	Near coast	At coast
1- to 3-yr RL	12.3	10.8	11.3	13.3
	16	14.3	14.6	15.6
	19.6	17	17.5	18
3- to 5-yr RL	16.5	12.8	12.4	15.3
	18	15.6	16.2	16.8
	20.1	17.5	18	19.6

are exceeded by three or more stations, we calculate the station-averaged wind speed and gradSLP for the associated storms. However, no correlation between the gradSLP and surface station winds for the multistation events was found. This null result is somewhat expected. The SLP gradient provides a proxy for the geostrophic forcing of the surface winds; however, as shown in Fink et al. (2009) and Durkee et al. (2012), the surface winds also contain ageostrophic components. Because the strong winds occur in the proximity of the cold front of the storms, it is also possible that momentum mixing associated with convection also provides an ageostrophic forcing for the surface winds (e.g., Booth et al. 2010).

5. Summary

This study identified historical strong wintertime surface wind events in the northeastern United States using station data. We applied methods from statistical extreme value theory to calculate probabilistic 1-, 3- and 5-yr return levels for surface weather stations and linked events that occurred on the same date to identify multistation events. Using these multistation strong wind events, the associated extratropical cyclones were identified. The main finding of the presented study is that storms approaching the region from the southwest are most likely to be associated with strong surface winds. Results of a track separation analysis of all cyclone tracks for 1979–2012 show that a storm causing strong surface winds is more likely to approach from the southwest than any other direction.

Our findings regarding the strongest winds within the warm sector support and expand on results from multiple studies over Europe (e.g., Leckebusch et al. 2008; Nissen et al. 2010). In particular, the present study confirms that for the northeastern United States, the Leckebusch et al. (2008) results regarding the relative location of the winds within the cyclone is the key for understanding the locations at which cyclones create strong winds. Additionally, we here utilized a new technique to identify strong synoptic wind events using station data: our multistation event approach. This technique is distinct from the wind-footprinting analysis that Leckebusch et al. (2008) and Nissen et al. (2010) applied to reanalysis winds. Therefore, the consistent results regarding the associated cyclones suggest that both methods (ours using surface observations and theirs using reanalysis winds) are capable of identifying strong synoptic windstorms. Future work will directly compare the two techniques.

To conclude, we discuss some of the implications of our results for storm impacts. First, if we consider storm impacts in the current climate, we can conclude that the extratropical cyclones that are associated with the strongest wind events over land most frequently are not the same as those that cause storm surge (i.e., northeasters), as reported in Dolan and Davis (1992). Next, if we consider storm impacts in a warmer world, the implications of our work suggest that projecting changes in surface wind events will depend foremost on the track of the cyclones. Based on the study of Colle et al. (2013), global climate models (GCMs) project an increase in cyclone tracks over the coastline and slightly inland. Based on our results, this suggests a possible increase in strong wind events if the GCM-projected track changes are correct.

Acknowledgments. The data used for this research were freely obtained from NOAA's National Climatic Data Center in the daily summary files of the integrated surface database and NOAA's National Weather Service in the form of storm reports as well as from ECMWF in the form of ERA-Interim via their Internet portals. We thank Kevin Hodges and Mike Bauer for sharing their cyclone-tracking code. James F. Booth, Dong Eun Lee, and Yochanan Kushnir were partially supported by the Consortium for Climate Risk in the Urban Northeast (Award NA10OAR4310212 from the NOAA RISA Program) and the Research Opportunities in Space and Earth Science ROSES-2012 NASA Grant NNX14AD48G.

REFERENCES

Ashley, W. S., and A. W. Black, 2008: Fatalities associated with nonconvective high-wind events in the United States. *J. Appl. Meteor. Climatol.*, **47**, 717–725, doi:10.1175/2007JAMC1689.1.

Asuma, J. V., 2010: Cool-season high-wind events in the Northeast U.S. M.S. thesis, Dept. of Atmospheric and Environmental Sciences, University at Albany, State University of New York, 117 pp. [Available online at http://cstar.cestm.albany.edu/CAP_Projects/Project17/JAsuma/Asuma_Total_4Oct10_Final.pdf.]

Bauer, M., and A. D. Del Genio, 2006: Composite analysis of winter cyclones in a GCM: Influence on climatological humidity. *J. Climate*, **19**, 1652–1672, doi:10.1175/JCLI3690.1.

Bengtsson, L., K. I. Hodges, and N. Keenlyside, 2009: Will extratropical storms intensify in a warmer climate? *J. Climate*, **22**, 2276–2301, doi:10.1175/2008JCLI2678.1.

Bernhardt, J. E., and A. T. DeGaetano, 2012: Meteorological factors affecting the speed of movement and related impacts of extratropical cyclones along the U.S. East Coast. *Nat. Hazards*, **61**, 1463–1472, doi:10.1007/s11069-011-0078-0.

Booth, J. F., L. Thompson, J. Patoux, K. A. Kelly, and S. Dickinson, 2010: The signature of the midlatitude tropospheric storm tracks in the surface winds. *J. Climate*, **23**, 1160–1174, doi:10.1175/2009JCLI3064.1.

——, C. Naud, and A. D. Del Genio, 2013: Diagnosing warm frontal cloud formation in a GCM: A novel approach using conditional subsetting. *J. Climate*, **26**, 5827–5845, doi:10.1175/JCLI-D-12-00637.1.

Born, K., P. L. Ludwig, and J. G. Pinto, 2012: Wind gust estimation for mid-European winter storms: Towards a probabilistic view. *Tellus*, **64A**, 17471, doi:10.3402/tellusa.v64i0.17471.

Browning, K. A., 2004: The sting at the end of the tail: Damaging winds associated with extratropical cyclones. *Quart. J. Roy. Meteor. Soc.*, **130**, 375–399, doi:10.1256/qj.02.143.

Casola, J. H., and J. M. Wallace, 2007: Identifying weather regimes in the 500-hPa geopotential height field for the Pacific–North American sector using a limited-contour clustering technique. *J. Appl. Meteor. Climatol.*, **46**, 1619–1630, doi:10.1175/JAM2564.1.

Catto, J. L., L. C. Shaffrey, and K. I. Hodges, 2010: Can climate models capture the structure of extratropical cyclones? *J. Climate*, **23**, 1621–1635, doi:10.1175/2009JCLI3318.1.

Coles, S., 2001: *An Introduction to Statistical Modeling of Extreme Values*. Springer, 209 pp.

——, and L. Pericchi, 2003: Anticipating catastrophes through extreme value modelling. *J. Roy. Stat. Soc.*, **52C**, 405–416, doi:10.1111/1467-9876.00413.

Colle, B. A., Z. Zhang, K. A. Lombardo, E. Chang, P. Liu, and M. Zhang, 2013: Historical evaluation and future prediction of eastern North American and western Atlantic extratropical cyclones in the CMIP5 models during the cool season. *J. Climate.* **26**, 6882–6903, doi:10.1175/JCLI-D-12-00498.1.

Davison, A. C., and R. L. Smith, 1990: Models for exceedances over high thresholds (with discussion). *J. Roy. Stat. Soc.*, **52B**, 393–442.

Dee, D. P., and Coauthors, 2011: The ERA-Interim reanalysis: Configuration and performance of the data assimilation system. *Quart. J. Roy. Meteor. Soc.*, **137**, 553–597, doi:10.1002/qj.828.

Della-Marta, P. M., and J. G. Pinto, 2009: Statistical uncertainty of changes in winter storms over the North Atlantic and Europe in an ensemble of transient climate simulations. *Geophys. Res. Lett.*, **36**, L14703, doi:10.1029/2009GL038557.

Dolan, R., and R. Davis, 1992: An intensity scale for Atlantic coast northeast storms. *J. Coastal Res.*, **8**, 840–853.

Donat, M. G., G. C. Leckebusch, J. G. Pinto, and U. Ulbrich, 2010: Examination of wind storms over central Europe with respect to circulation weather types and NAO phases. *Int. J. Climatol.*, **30**, 1289–1300, doi:10.1002/joc.1982.

Durkee, J. D., C. F. Fuhrmann, J. A. Knox, and J. D. Frye, 2012: Ageostrophic contributions to a non-convective high wind event in the Great Lakes region. *Natl. Wea. Dig.*, **36**, 28–41.

Fink, A. H., T. Brucher, V. Ermert, A. Kruger, and J. G. Pinto, 2009: The European storm Kyrill in January 2007: Synoptic evolution, meteorological impacts and some considerations with respect to climate change. *Nat. Hazards Earth Syst. Sci.*, **9**, 405–423, doi:10.5194/nhess-9-405-2009.

Gatzen, C., T. Púčik, and D. Ryva, 2011: Two cold-season derechoes in Europe. *Atmos. Res.*, **100**, 740–748, doi:10.1016/j.atmosres.2010.11.015.

Haas, R., and J. G. Pinto, 2012: A combined statistical and dynamical approach for downscaling large-scale footprints of European windstorms. *Geophys. Res. Lett.*, **39**, L23804, doi:10.1029/2012GL054014.

Hayes, J. C., and S. C. Kuhl, 1995: An initial comparison of manual and automated surface observing system observations at the Atlantic City, New Jersey International Airport, NOAA Tech. Memo. NWS ER-89, 26 pp. [Available online at http://docs.lib.noaa.gov/noaa_documents/NWS/NWS_ER/TM_NWS_ER_89.pdf.]

He, Y., A. H. Monahan, C. G. Jones, A. Dai, S. Biner, D. Caya, and K. Winger, 2010: Probability distributions of land surface wind speeds over North America. *J. Geophys. Res.*, **115**, D04103, doi:10.1029/2008JD010708.

Hirsch, M., A. T. DeGaetano, and S. J. Colucci, 2001: An East Coast winter storm climatology. *J. Climate*, **14**, 882–899, doi:10.1175/1520-0442(2001)014<0882:AECWSC>2.0.CO;2.

Hodges, K. I., 1999: Adaptive constraints for feature tracking. *Mon. Wea. Rev.*, **127**, 1362–1373, doi:10.1175/1520-0493(1999)127<1362:ACFFT>2.0.CO;2.

——, R. W. Lee, and L. Bengtsson, 2011: A comparison of extratropical cyclones in recent reanalyses ERA-Interim, NASA MERRA, NCEP CFSR, and JRA-25. *J. Climate*, **24**, 4888–4906, doi:10.1175/2011JCLI4097.1.

Iacopelli, A. J., and J. A. Knox, 2001: Mesoscale dynamics of the record-breaking 10 November 1998 mid-latitude cyclone: A satellite-based case study. *Natl. Wea. Dig.*, **25**, 33–42.

Knippertz, P., U. Ulbrich, and P. Speth, 2000: Changing cyclones and surface wind speeds over the North Atlantic and Europe in a transient GHG experiment. *Clim. Res.*, **15**, 109–122, doi:10.3354/cr015109.

Knox, J. A., J. D. Frye, J. D. Durkee, and C. M. Fuhrmann, 2011: Non-convective high winds associated with extratropical cyclones. *Geogr. Compass*, **5**, 63–89, doi:10.1111/j.1749-8198.2010.00395.x.

Kunkel, K. E., D. R. Easterling, D. A. R. Kristovich, B. Gleason, L. Stoecker, and R. Smith, 2012: Meteorological causes of the secular variations in observed extreme precipitation events for the conterminous United States. *J. Hydrometeor.*, **13**, 1131–1141, doi:10.1175/JHM-D-11-0108.1.

——, and Coauthors, 2013: Monitoring and understanding trends in extreme storms: State of knowledge. *Bull. Amer. Meteor. Soc.*, **94**, 499–514, doi:10.1175/BAMS-D-11-00262.1.

Lacke, M. C., J. A. Knox, J. D. Frye, A. E. Stewart, J. D. Durkee, C. M. Fuhrmann, and S. M. Dillingham, 2007: A climatology of cold-season nonconvective wind events in the Great Lakes region. *J. Climate*, **20**, 6012–6022, doi:10.1175/2007JCLI1750.1.

Leckebusch, G. C., D. Renggli, and U. Ulbrich, 2008: Development and application of an objective storm severity measure for the northeast Atlantic region. *Meteor. Z.*, **17**, 575–587, doi:10.1127/0941-2948/2008/0323.

Ludwig, P., J. G. Pinto, S. A. Hoepp, A. H. Fink, and S. L. Gray, 2015: Secondary cyclogenesis along an occluded front leading to damaging wind gusts: Windstorm Kyrill, January 2007. *Mon. Wea. Rev.*, **143**, 1417–1437, doi:10.1175/MWR-D-14-00304.1.

McKee, T. B., N. J. Doesken, C. A. Davey, and R. A. Pielke Sr., 2000: Climate data continuity with ASOS: Report for period April 1996 through June 2000. Colorado Climate Center Climatology Rep. 00-3, 82 pp.

Miller, J. E., 1946: Cyclogenesis in the Atlantic coastal region of the United States. *J. Meteor.*, **3**, 31–44, doi:10.1175/1520-0469(1946)003<0031:CITACR>2.0.CO;2.

Neu, U., and Coauthors, 2013: IMILAST: A community effort to intercompare extratropical cyclone detection and tracking

algorithms. *Bull. Amer. Meteor. Soc.*, **94**, 529–547, doi:10.1175/BAMS-D-11-00154.1.

Nissen, K. M., G. C. Leckebusch, J. G. Pinto, D. Renggli, S. Ulbrich, and U. Ulbrich, 2010: Cyclones causing wind storms in the Mediterranean: Characteristics, trends and links to large-scale patterns. *Nat. Hazards Earth Syst. Sci.*, **10**, 1379–1391, doi:10.5194/nhess-10-1379-2010.

Niziol, T. A., and T. J. Paone, 2000: A climatology of non-convective high wind events in western New York state. NOAA Tech. Memo. NWS ER-91, 36 pp. [Available online at http://www.erh.noaa.gov/er/hq/ssd/erps/tm/tm91.pdf.]

Pfahl, S., 2014: Characterising the relationship between weather extremes in Europe and synoptic circulation features. *Nat. Hazards Earth Syst. Sci.*, **14**, 1461–1475, doi:10.5194/nhess-14-1461-2014.

Pickands, J., 1975: Statistical-inference using extreme order statistics. *Ann. Stat.*, **3**, 119–131, doi:10.1214/aos/1176343003.

Pinto, J. G., E. L. Fröhlich, G. C. Leckebusch, and U. Ulbrich, 2007: Changing European storm loss potentials under modified climate conditions according to ensemble simulations of the ECHAM5/MPI-OM1 GCM. *Nat. Hazards Earth Syst. Sci.*, **7**, 165–175, doi:10.5194/nhess-7-165-2007.

——, M. K. Karreman, K. Born, P. M. Della-Marta, and M. Klawa, 2012: Loss potentials associated with European windstorms under future climate conditions. *Climate Res.*, **54**, 1–20, doi:10.3354/cr01111.

Pryor, S. C., and Coauthors, 2009: Wind speed trends over the contiguous United States. *J. Geophys. Res.*, **114**, D14105, doi:10.1029/2008JD011416.

——, R. Conrick, C. Miller, J. Tytell, and R. J. Barthelmie, 2014: Intense and extreme wind speeds observed by anemometer and seismic networks: An eastern U.S. case study. *J. Appl. Meteor. Climatol.*, **53**, 2417–2429, doi:10.1175/JAMC-D-14-0091.1.

Reitan, C. H., 1974: Frequencies of cyclones and cyclogenesis for North America, 1951–1970. *Mon. Wea. Rev.*, **102**, 861–868, doi:10.1175/1520-0493(1974)102<0861:FOCACF>2.0.CO;2.

Ribatet, M., 2007: POT: Modelling peaks over a threshold. *R News*, No. 7(1), 34–36. [Available online at http://cran.r-project.org/doc/Rnews/Rnews_2007-1.pdf.]

Roberts, J. F., and Coauthors, 2014: The XWS open access catalogue of extreme European windstorms from 1979 to 2012. *Nat. Hazards Earth Syst. Sci.*, **14**, 2487–2501, doi:10.5194/nhess-14-2487-2014.

Schwierz, C., P. Köllner-Heck, E. Zenklusen Mutter, D. N. Bresch, P.-L. Vidale, M. Wild, and C. Schär, 2010: Modelling European winter wind storm losses in current and future climate. *Climatic Change*, **101**, 485–514, doi:10.1007/s10584-009-9712-1.

Seregina, L. S., R. Haas, K. Born, and J. G. Pinto, 2014: Development of a wind gust model to estimate gust speeds and their return periods. *Tellus*, **66A**, 22905, doi:10.3402/tellusa.v66.22905.

Smith, A., N. Lott, and R. Vose, 2011: The integrated surface database: Recent developments and partnerships. *Bull. Amer. Meteor. Soc.*, **92**, 704–708, doi:10.1175/2011BAMS3015.1.

Ulbrich, U., A. H. Fink, M. Klawa, and J. G. Pinto, 2001: Three extreme storms over Europe in December 1999. *Weather*, **56**, 70–80, doi:10.1002/j.1477-8696.2001.tb06540.x.

Vose, R. S., and Coauthors, 2014: Monitoring and understanding changes in extremes: Extratropical storms, winds, and waves. *Bull. Amer. Meteor. Soc.*, **95**, 377–386, doi:10.1175/BAMS-D-12-00162.1.

Ward, J. H., Jr., 1963: Hierarchical grouping to optimize an objective function. *J. Amer. Stat. Assoc.*, **58**, 236–244, doi:10.1080/01621459.1963.10500845.

Yarnal, B., 1993: *Synoptic Climatology in Environmental Analysis: A Primer.* Belhaven Press, 105 pp.